Available online at www.sciencedirect.com
ScienceDirect
Scripta Materialia 61 (2009) 265–268
Scripta MATERIALIA
www.elsevier.com/locate/scriptamat

Effects of Cu ion irradiation in $Cu_{50}Zr_{45}Ti_5$ metallic glass

Jesse Carter,[a] E.G. Fu,[b] Michael Martin,[a] Guoqiang Xie,[c] X. Zhang,[b] Y.Q. Wang,[d] D. Wijesundera,[e] X.M. Wang,[e] Wei-Kan Chu[e] and Lin Shao[a,*]

[a]*Department of Nuclear Engineering, Texas A&M University, College Station, TX 77843, USA*
[b]*Department of Mechanical Engineering, Texas A&M University, College Station, TX 77843, USA*
[c]*Institute for Materials Research, Tohoku University, Sendai 980-8577, Japan*
[d]*Los Alamos National Laboratory, Los Alamos, NM 87545, USA*
[e]*Texas Center for Superconductivity and Department of Physics, University of Houston, Houston, TX 77204, USA*

Received 9 March 2009; revised 28 March 2009; accepted 29 March 2009
Available online 5 April 2009

We studied the role of thermal spike in nanocrystallization of $Cu_{50}Zr_{45}Ti_5$ metallic glasses after 1 MeV Cu ion irradiation at room temperature. Nanocrystals of $Cu_{10}Zr_7$ and $CuZr_2$ phases are formed after the ion irradiation. The study suggests that thermal spike formation and subsequent quenching are too fast to allow direct structural transformation in the damage cascade regions. The overall irradiation effects are caused by enhanced atomic mobility due to increased excessive free volume.

Keywords: Metallic glass; Ion irradiation; Crystallization

Metallic glasses (MGs) have been a subject of great interest during the past decades because of their unique mechanical and chemical properties. Due to a lack of crystalline structures and grain boundaries, MGs exhibit extremely high hardness and superior resistance to corrosion [1–7], but their low ductility hinders industrial applicability. Following the recognition that introducing nanocrystals into MGs can enhance ductility, the study on partial crystallization of MGs has proliferated. Numerous studies have shown that nanocrystal formation can be induced by annealing [8], deformation [9], bending [10], nanoindentation [11], and ion and electron irradiation [12–16]. Upon ion/electron irradiation, if energy transfer is large enough, target atoms will be displaced from their initial sites. This creates vacancy-like defects and increases excessive free volume in the system [13–16]. Based on free-volume model developed by Cohen and Turnbull [17], and later by Spaepen [18], particle irradiation is expected to enhance atomic mobility, leading to short-range order and, finally, crystallization. The above theory has been supported by a recent atomic scale simulation [19], which shows that atoms around the displaced region have transient enhanced mobility on a short time scale, and the whole sample experiences mobility enhancement due to the diffusion of the excessive free volume on a longer time scale. However, the level of understanding of the underlying mechanisms is still rather limited. One question to be addressed is the effect of thermal spikes on nanocrystal formation.

Violent nucleus–nucleus collisions can create displacement cascades and thermal spikes. The core of the cascade is vacancy rich and retains enough energy to cause melting and resolidification [20]. The radius of the collision cascade is usually a few nanometers or less. With such localized high-temperature heating, nanocrystals might form in a way different from low temperature thermal annealing. High-energy Cu ion irradiation on $Cu_{50}Zr_{45}Ti_5$ metallic glass has been performed in this study to gain understanding of the nature of nanocrystal formation by ion irradiation. The self ion irradiation eliminates complexity caused by impurities. The $Cu_{50}Zr_{45}Ti_5$ MG was selected in the present study due to its attractive mechanical property and the fact that its crystallization kinetics has been well studied [21].

Our studies began with preparing $Cu_{50}Zr_{45}Ti_5$ metallic glass ribbon samples by rapid solidification. Samples were measured to be 20 μm in thickness and 1.5 mm in width. As-spun samples were irradiated with 1 MeV Cu ions to a total fluence of $1 \times 10^{16}/cm^2$ at room

* Corresponding author. Tel.: +1 9798454107; fax: +1 9798456443; e-mail: lshao@mailaps.org

1359-6462/$ - see front matter © 2009 Acta Materialia Inc. Published by Elsevier Ltd. All rights reserved.
doi:10.1016/j.scriptamat.2009.03.060

temperature using a NEC 1.7 MeV tandem accelerator. The beam current was controlled to be ~100 nA cm^{-2} and the beam heating on the irradiated samples was measured to be less than 50 °C. The projected range of 1 MeV Cu in the glass is around 460 nm [22]. Samples were characterized using Bruker-AXS D8 VARIO high-resolution X-ray diffractometer. Transmission electron microscopy (TEM) and high-resolution TEM were performed by using a JEOL 2010 microscope equipped with Gatan SC1000 ORIUS CCD camera, operated at 200 kV. TEM specimens were prepared on a Fischione 1010 ion mill using 2 keV Ar ions while the sample was cooled by a liquid nitrogen cooling system. The specimens were slowly rotated during thinning to avoid inhomogeneous etching. Our recent studies have shown that the above specimen preparation procedure can avoid ion-milling-induced microstructural changes [23].

Figure 1 shows X-ray diffraction (XRD) spectra of the as-spun and irradiated ribbon $Cu_{50}Zr_{45}Ti_5$ glasses. For the as-spun sample (gray color) a broad peak is presented, which is typical for the glassy state. For the irradiated sample (dark color), the XRD spectrum shows sharp peaks and suggests the presence of crystalline phases. Several diffraction peaks corresponding to crystallographic planes from $Cu_{10}Zr_7$ and $CuZr_2$ phases are marked in Figure 1. However, TEM characterization is needed for more conclusive determination of crystalline phases since both spectra in Figure 1 are noisy due to relatively high detection limits of XRD.

Figure 2a shows a typical bright-field TEM micrograph from the Cu-irradiated sample. Precipitation and dark particles are presented. The corresponding SAD pattern shows white diffraction dots and sharp rings, indicating long-range order and the nucleation of nanocrystals. For a comparison, Figure 2b shows a typical dark-field TEM micrograph obtained from the same sample. It reveals the presence of nanocrystalline particles. Systematic comparison between a series of bright-field and dark-field micrographs suggests that the dark particles observed in bright-field TEM micrographs are indeed nanocrystals.

Figure 3 plots the size distribution of nanocrystals. Nanocrystal diameters range mostly from 2 to 14 nm, with a typical size of 6 nm. The inset in Figure 3 is a high-resolution TEM micrograph of the Cu-irradiated sample. Crystalline structures inside nanoparticles are clearly visible. As we will discuss below, these nanocrystals are either $Cu_{10}Zr_7$ (primary) or $CuZr_2$ phases.

Figure 4 shows the enlarged SAD pattern obtained from the Cu-irradiated sample. The interplanar distances calculated from the SAD pattern were compared with those from database and are summarized in Table 1. Single crystal (100) was used for calibration. The extracted *d*-spacing values suggest the formation of $Cu_{10}Zr_7$ (primary) and $CuZr_2$ (minor) phases. Crystallographic planes from these two phases are labeled in the SAD pattern. The body-centered cubic CuZr phase with *d*-spacings of 2.307, 1.883, 1.631, 1.459, 1.332 and

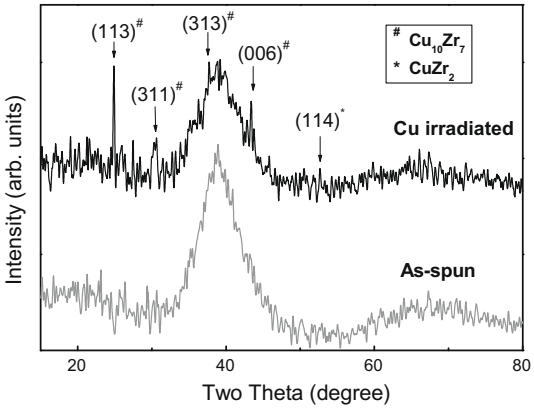

Figure 1. XRD patterns of as-spun and Cu ion irradiated $Cu_{50}Zr_{45}Ti_5$ metallic glass. Diffraction peaks from crystalline $Cu_{10}Zr_7$ (#) and $CuZr_2$ (*) phases are marked.

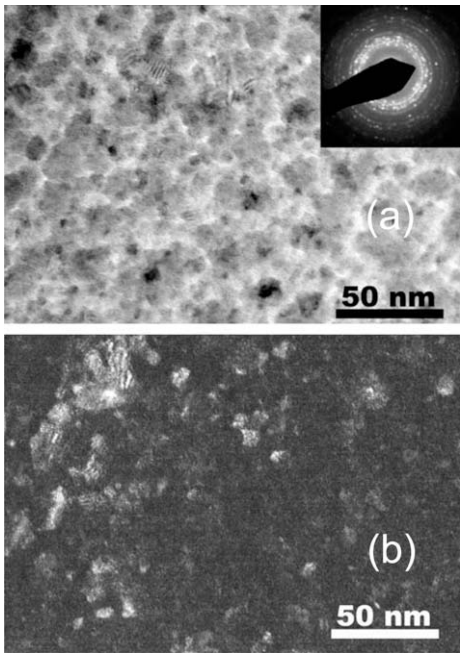

Figure 2. (a) Bright-field TEM micrograph and the corresponding SAD pattern inset of Cu-ion-irradiated $Cu_{50}Zr_{45}Ti_5$ glass specimen, and (b) dark-field TEM micrograph of the same sample.

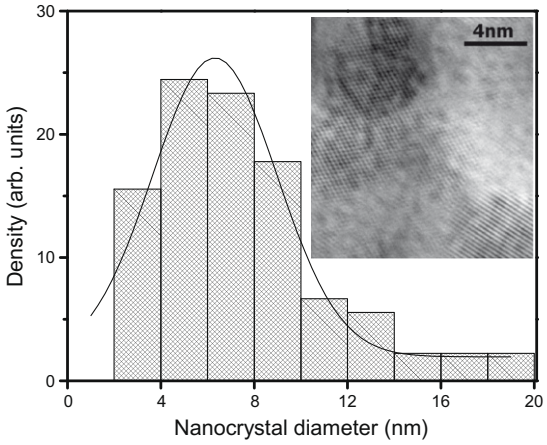

Figure 3. Size distribution of nanocrystals in Cu ion irradiated $Cu_{50}Zr_{45}Ti_5$, estimated from TEM micrographs. The inset is a high-resolution TEM micrograph.

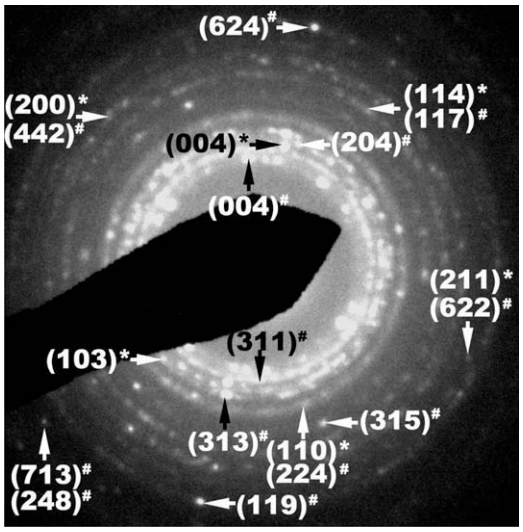

Figure 4. The SAD pattern of Cu ion irradiated $Cu_{50}Zr_{45}Ti_5$ glass. The Miller indices correspond to crystalline $Cu_{10}Zr_7$ (#) and $CuZr_2$ (*) phases.

Table 1. Comparison of *d*-spacing (in angstroms) from the present study and from a database [24].

Experimental data from the present study	$Cu_{10}Zr_7$ standard *d*-spacing/orientation	$CuZr_2$ standard *d*-spacing/orientation
3.178	3.174/(004)	
2.889	2.880/(311)	
2.755		2.782/(004)
2.642	2.621/(204)	
2.463		2.429/(103)
2.416	2.420/(313)	
2.252	2.287/(224)	2.269/(110)
1.933	1.923/(315)	
1.759	1.746/(117)	1.761/(114)
1.603	1.598/(442)	1.607/(200)
1.433	1.437/(662)	1.429/(211)
1.372	1.378/(119)	
1.260	1.262/(248),(713)	
1.116		1.117/(010)
1.035		1.030/(303)

1.153 Å, and others, could not be identified [24]. Our particular interest in CuZr phase is due to the reason that this phase is expected to form at a temperature comparable to thermal spikes [25].

Structures of $Cu_{10}Zr_7$, $CuZr_2$ and CuZr crystals are very different. $Cu_{10}Zr_7$ has a complex unit cell containing 68 atoms over nine inequivalent sites [26]. $CuZr_2$ has an $MoSi_2$-type structure with a tetragonal cell containing six atoms [27]. As the simplest structure, CuZr has a CsCl-type structure, but it is metastable at low temperature. Stable CuZr phase forms only at a temperature >985 K [25]. In one previous study, an initially amorphous Zr_xCu_{1-x} alloy was continuously heated from low temperature to high temperature. $Cu_{10}Zr_7$ and $CuZr_2$ phases are observed but no CuZr phase can be identified [28]. In another study, if a liquid melt of Zr–Cu–Al was cooled from high temperature to low temperature, CuZr phase was observed in the region with a high cooling rate, while in the region with a low cooling rate $Cu_{10}Zr_7$ and $CuZr_2$ phases were identified [29]. Therefore, a metastable CuZr phase will form if cooling is fast. Otherwise, it will decompose into more stable $Cu_{10}Zr_7$ and $CuZr_2$ phases.

The damage cascades caused by ion irradiation will typically last for a period of 10^{-13} s. After that, a localized melting zone due to thermal spike formation is left. The highly localized heating typically lasts for a period of 10^{-12} s. Considering the critical cooling rates to form MG for Cu–Zr alloys in the range of 4.3×10^2–3.6×10^4 K s^{-1} and, for Cu–Zr–Ti alloys, 6×10^3–1.4×10^4 K s^{-1} [30], the quenching rate of a thermal spike is much faster than the critical cooling rate. This fact leads to the following two possibilities: (i) if damage cascades do not cause decomposition, MG in the cascade core region will keep its original composition and ultra fast quenching of a thermal spike will not lead to nanocrystal formation; (ii) if CuZr phase actually forms in the thermal spike region, the ultrafast quenching of the thermal spike should keep metastable CuZr phase (or at least part of it) at ambient temperature, according to Ref. [28]. Based on the above discussion and the fact that no CuZr phase is observed after Cu irradiation, we hypothesized that CuZr phase does not form in the damage cascade region.

Early studies by Meldrum et al. [31] have shed light into the complexity of irradiation-induced crystallization. These authors reported evidence of a transient liquid-like phase caused by displacement cascades in solids. Under high-temperature irradiation, new crystalline phases were formed in zircon. Such phases were not observed under low-temperature irradiation. The difference was explained due to different quenching rates: a high quenching rate occurs at low ambient temperature and does not allow sufficient time for nucleation of new phase [31]. A similar mechanism might apply in the present study, even though the materials are different.

The present study suggests that the quenching rate of thermal spike is so high that it becomes difficult to achieve short-range order in the damage cascade region. In order to form a nucleation site, the magnitude of the necessary diffusion coefficient within the displacement cascade region can be estimated by $D = x^2/t$. If $x \approx 1$ nm and $t \approx 1$ ps, then $D = 1 \times 10^{-6}$ m$^2/s$. It is unlikely that the atomic diffusivity of $Cu_{50}Zr_{45}Ti_5$ at thermal spike temperature can be that high, considering groups of atoms need to jump collectively [32]. Recently, self-diffusion in a binary $Cu_{33}Zr_{67}$ glass has been modeled by molecular dynamics simulation [33]. It shows that, at a melting temperature of 2000 K, Cu diffusivity is 4×10^{-9} m^2 s^{-1}, which is a few orders of magnitude lower than the above-estimated diffusivity to form the necessary solute segregation. Although $Cu_{33}Zr_{67}$ is different from the $Cu_{50}Zr_{45}Ti_5$ studied here, both materials have similar packing density and nearest atomic distance, and their self-diffusion coefficients should be comparable.

Recently, the mechanism of shear-band-formation-induced nanocrystallization has been investigated [34]. The phenomenon is different from what happens in ion irradiation. The amount of energy deposited by shear band formation is much larger, the energy dissipation takes longer and the region being heated is wider [34]. Thus, nanocrystals can be formed in the vicinity of the shear bands. As discussed in the preceding paragraphs, fast quenching of

the thermal spike in ion irradiated samples makes correlated atomic movements difficult. Rather than directly causing phase transformation, quenching spreads excessive free volume over a large region. This enhances atomic mobility and leads to increased short-range order and subsequent nucleation at longer times.

For applications, ion irradiation can be used as a method to improve materials' mechanical properties. Since irradiation temperature, implanted ion species, ion energy, ion flux and fluency can be well controlled, the technique can achieve adjustable nanocrystallization and increase both hardness and ductility of MGs with high repeatability. In addition, ion implantation of impurities into MG can increase thermodynamic stabilities. One previous study has shown that implantation of Co into ZrCuNiAl alloy can lower its glass transition temperature and enlarge the supercooled liquid range [35]. Introducing impurities is expected to also increase nucleation sites. Since the activation energy for nucleation is usually larger than the activation energy for crystal growth in metallic glasses [36], a technique combining ion implantation to introduce nucleation sites and annealing to induce nanocrystal growth might achieve optimized nanocrystallization at low temperatures. However, ion implantation is a surface modification technique. The structural changes are limited by ions' penetration depth. Thus, the technique is useful to improve surface properties but has its limitation to improve MG's machinability.

In summary, 1 MeV Cu ion irradiation of $Cu_{50}Zr_{45}Ti_5$ metallic glass was found to induce nanocrystalline $Cu_{10}Zr_7$ and $CuZr_2$ phases. However, CuZr phase, a decomposition product expected with high-temperature annealing, is not observed after ion irradiation. The study suggests that nanocrystal formation is due to enhanced atomic mobility caused by the introduction of excessive free volume brought on by ion irradiation. It seems unlikely that the decomposition is due to a localized structural transformation in the damage cascade and thermal spike region.

This work was financially supported by the University Embryonic Technologies Program from Siemens Power Generation Emerging Technologies. L.S. would like to acknowledge the support from the NRC Early Career Development Grant. X.Z. acknowledges the support by DOE under Grant No. DE-FC07-05ID14657. This work was performed, in part, at the Center for Integrated Nanotechnologies, a DOE-supported user facility. The University of Houston group is supported by the State of Texas through the Texas Center for Superconductivity at the University of Houston, and through the DOE under Grant No. DE-FG02-05ER46208

[1] A. Inoue, Acta Mater. 48 (2000) 279.
[2] A. Peker, W.L. Johnson, Appl. Phys. Lett. 63 (1993) 2342.
[3] W.L. Johnson, MRS Bull. 24 (1999) 42.
[4] M.F. Ashby, A.L. Greer, Scr. Mater. 54 (2006) 321.
[5] A.I. Salimon, Mater. Sci. Eng. A 375 (2004) 385.
[6] A.L. Greer, Science 267 (1995) 1947.
[7] A. Peker, W.L. Johnson, Appl. Phys. Lett. 63 (1993) 2343.
[8] X.Y. Jiang, Z.C. Zhong, A.L. Greer, Mater. Sci. Eng. A 789 (1997) 226.
[9] R. Schulz, M.L. Trudeau, D. Dussault, A. Van Neste, J. Phys. 51 (1990) C4259.
[10] H. Chen, Y. He, G.J. Shiflet, S.J. Poon, Nature 367 (1994) 6463.
[11] J.-J. Kim, Y. Choi, S. Suresh, A.S. Argon, Science 295 (2002) 654.
[12] J. Carter, E.G. Fu, G. Bassiri, B.M. Dvorak, N.D. Theodore, G.Q. Xie, D.A. Lucca, M. Martin, M. Hollander, X. Zhang, L. Shao, Nucl. Instru. Meth. B (2009), doi: 10.1016/j.nimb.2009.01.081.
[13] X.W. Du, M. Takeguchi, M. Tanaka, K. Furuya, Appl. Phys. Lett. 82 (2003) 1108.
[14] T. Nagase, Y. Umakoshi, Mater. Trans. 46 (2005) 616.
[15] G.Q. Xie, Q. Zhang, D.V. Louzguine-Luzgin, W. Zhang, A. Inoue, Mater. Trans. 47 (2006) 1930.
[16] E.G. Fu, J. Carter, M. Martin, G.Q. Xie, X. Zhang, Y.Q. Wang, R. Littleton, L. Shao, Scripta Mater. 61 (2009) 40.
[17] M.H. Cohen, D. Turnbull, J. Chem. Phys. 31 (1959) 1164.
[18] F. Spaepen, in: J.J. Poirier, M. Kleman (Eds.), Les Houches Lectures on Physics of Defects, Amsterdam, North Holland, 1981.
[19] V. Rosato, F. Cleri, J. Non-Cryst. Solids 144 (1992) 187.
[20] M. Nastasi, J.W. Mayer, J.K. Hirvonen, Ion–Solid Interactions: Fundamentals and Applications, Cambridge University Press, New York, 1996.
[21] G.Q. Xie, D.V. Louzguine-Luzgin, Q. Zhang, W. Zhang, A. Inoue, J. Alloys Compd. (2008), doi: 10.1016/j.jallcom.2008.07.191.
[22] The stopping and range of ions in matter (SRIM) simulation. Available from: <www.srim.org>.
[23] E.G. Fu, Jesse Carter, Michael Martin, Guoqiang Xie, X. Zhang, Y.Q. Wang, Rick Littleton, Lin Shao, unpublished data.
[24] Available from: <www.icdd.com>.
[25] E.M. Carvalho, I.R. Harris, J. Mater. Sci. 15 (1980) 1224.
[26] P. Garoche, J. Bigot, Phys. Rev. B 28 (1983) 6886.
[27] M. Nevitt, I.V. Downey, Trans. AIME 224 (1962) 195.
[28] H.R. Wang, Y.F. Ye, Z.Q. Shi, X.Y. Teng, G.H. Min, J. Non-Cryst. Solids 311 (2002) 36.
[29] Y.F. Sun, B.C. Wei, Y.R. Wang, W.H. Li, T.L. Cheung, C.H. Shek, Appl. Phys. Lett. 87 (2005) 051905.
[30] L. Ge, X. Hui, E.R. Wang, G.L. Chen, R. Arroyave, Z.K. Liu, Intermetallics 16 (2008) 27.
[31] A. Meldrum, S.J. Zinkle, L.A. Boatner, R.C. Ewing, Nature 395 (1998) 56.
[32] C. Gaukel, M. Kluge, H.R. Schober, Phil. Mag. B 79 (1999) 1907.
[33] M. Kluge, H.R. Schober, J. Non-Cryst. Solids 352 (2006) 5093.
[34] D.T.A. Matthews, V. Ocelík, P.M. Bronsveld, J.Th.M. De Hosson, Acta Mater. 56 (2008) 1762.
[35] P.J. Tao, Y.Z. Yang, X.J. Bai, Z.X. Mu, G.Q. Li, Z.W. Xie, X.C. Chen, Surf. Coat. Technol. 203 (2009) 1656.
[36] K. Lu, J.T. Wang, Mater. Sci. Eng. A 133 (1991) 500.